JACS
JOURNAL OF THE AMERICAN CHEMICAL SOCIETY
Article
pubs.acs.org/JACS

Structure and Composition of Insulin Fibril Surfaces Probed by TERS

Dmitry Kurouski,[†] Tanja Deckert-Gaudig,[‡] Volker Deckert,[‡,§] and Igor K. Lednev*[,†]

[†]University at Albany, State University of New York, 1400 Washington Avenue, Albany, New York 12222, United States
[‡]Institute of Photonic Technology, Albert-Einstein-Strasse 9, Jena, Germany 07745
[§]Institute for Physical Chemistry, University of Jena, Helmholtzweg 4, Jena, Germany 07743

Supporting Information

ABSTRACT: Amyloid fibrils associated with many neurodegenerative diseases are the most intriguing targets of modern structural biology. Significant knowledge has been accumulated about the morphology and fibril-core structure recently. However, no conventional methods could probe the fibril surface despite its significant role in the biological activity. Tip-enhanced Raman spectroscopy (TERS) offers a unique opportunity to characterize the surface structure of an individual fibril due to a high depth and lateral spatial resolution of the method in the nanometer range. Herein, TERS is utilized for characterizing the secondary structure and amino acid residue composition of the surface of insulin fibrils. It was found that the surface is strongly heterogeneous and consists of clusters with various protein conformations. More than 30% of the fibril surface is dominated by β-sheet secondary structure, further developing Dobson's model of amyloid fibrils (Jimenez et al. *Proc. Natl. Acad. Sci. U.S.A.* **2002**, *99*, 9196−9201). The propensity of various amino acids to be on the fibril surface and specific surface secondary structure elements were evaluated. β-sheet areas are rich in cysteine and aromatic amino acids, such as phenylalanine and tyrosine, whereas proline was found only in α-helical and unordered protein clusters. In addition, we showed that carboxyl, amino, and imino groups are nearly equally distributed over β-sheet and α-helix/unordered regions. Overall, this study provides valuable new information about the structure and composition of the insulin fibril surface and demonstrates the power of TERS for fibril characterization.

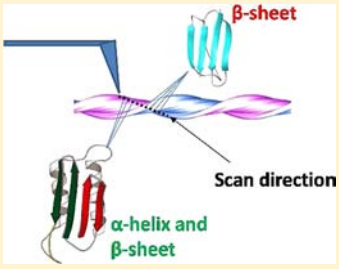

INTRODUCTION

Amyloid fibrils are β-sheet-rich protein aggregates that are commonly found in intracellular and extracellular deposits associated with various neurodegenerative diseases, such as Alzheimer's, Parkinson's, and prion diseases.[1] Amyloid deposits have also been found in many other maladies, including type-II diabetes, prolactoma, and primary amyloidosis.[2−4] Many of these diseases, such as injection amyloidosis and insulinoma, are associated with insulin aggregation.[5]

Determining the structural organization of amyloid fibrils has been one of the most intriguing problems in structural biology in recent decades.[6] This problem is challenging because amyloid fibrils are noncrystalline and insoluble. Thus, the application of classical structural biology tools, such as X-ray crystallography and solution NMR, is limited.[7,8] Solid-state NMR, which requires site-specific isotope labeling, has been used to determine the structure of amyloid-β (Aβ)[9] and transthyretin (TTR)[10] fibrils. Raman spectroscopy including normal[11,12] and ultraviolet resonance Raman[13] spectroscopy has been used to characterize the fibril structure. These techniques report, on average, bulk properties dominated by the contribution from the fibril core. Tip-enhanced Raman scattering (TERS) offers a high depth and lateral spatial resolution in the nanometer range due to a strong field enhancement by a metalized tip of an atomic force microscope (AFM) coupled to a Raman spectrometer.[14−16] TERS has been used to investigate the surface organization of eukaryotic cells and viruses.[17−19] We have recently demonstrated a great potential of TERS for structural characterization of amyloid fibrils.[20]

Herein, we report the characterization of insulin fibril surfaces, including secondary structural composition and the distribution of amino acid residues. The secondary structure of the fibril surface is very heterogeneous and contains areas with varying amounts of β-sheet, α-helical, and unordered protein conformations. However, α-helical/unordered regions dominate the fibril surface. Approximately 34% of all of the collected spectra indicate the presence of β-sheet structure. This discovery further develops Dobson's model of amyloid fibrils,[21] which suggests that a significant part of the fibril core is not covered by unordered and α-helical protein segments. In addition, we evaluated the propensity of phenylalanine (Phe), tyrosine (Tyr), cysteine (Cys), proline (Pro) and histidine (His) to form various protein secondary structures on the fibril surface. Some amino acids were preferentially located in areas dominated by a specific type of protein secondary structure.

MATERIALS AND METHODS

Bovine insulin (Sigma-Aldrich, St. Louis, MO) was dissolved (60 mg/mL) in HCl, pH 2.5. The protein solution was heated at 70 °C for 2.5 h without stirring. Immediately after fibrillation was complete, an aliquot of the fibrillar gel was resuspended in HCl (pH 2.5) solution with a 1:100 dilution factor (v/v). A drop of this solution was placed onto a precleaned glass.[22] After the surface was exposed to the solution

Received: April 10, 2012
Published: July 19, 2012

 © 2012 American Chemical Society

for 2−3 min, the solution excess was gently removed, and the surface was rinsed with HCl (pH 2.5) solution and dried under an argon flow.

Tip-enhanced Raman spectra and fibril AFM images were acquired on a Nanowizard I (JPK Instruments AG, Germany) mounted on an inverted microscope (Olympus IX70, Japan). The following conditions were used: oil immersion objective, 60×, NA = 1.45 (Olympus, Japan); mounted on a Piezo (PIFOC, Physik Instrumente, Germany) synchronizing the *z*-movement of the TERS tip and the laser focus; a confocal Raman spectrometer (LabRam HR, Horiba Jobin Yvon, France) with a liquid nitrogen-cooled CCD camera (ISA Spectrum One, Horiba Jobin Yvon, France), a krypton ion laser (Innova 300c, wavelength 530,9 nm, U.S.A.) as the excitation source. Each TERS spectrum was accumulated for 10 s. Spectra were collected from the fibril surface with a lateral distance step that varied from 0.5 to 10 nm. The lateral steps were controlled by an additional 100 μm × 100 μm sample scanning stage (P-734, Physik Instrumente, Germany). To confirm that the TERS tip was not contaminated during the acquisition of spectra of the fibril surface, a reference spectrum from the glass slide was recorded at the end of each measurement. Selected AFM topography images are shown in the Supporting Information (SI), Figures S1. GRAMS/AI 7.0 (Thermo Galactic, Salem, NH) was used for spectral data processing. Spectra shown are raw spectra, no smoothing or baseline correction was applied, indicating the high quality of the TERS data.

Scanning Electron Microscopy (SEM). An aliquot of diluted fibril solution was deposited on a 200-mesh copper grid. After the grid was exposed to the solution for 2−3 min, the excess of remaining solution was gently removed. A drop of 1% uranyl acetate (Sigma-Aldrich, St. Louis, MO) was placed on the copper grid and exposed on its surface for 1 min. Finally, the grid was dried under room temperature prior to SEM imaging. The samples were imaged on a Zeiss Supra 55 SEM in InLense mode with 5 kV EHT.

RESULTS

Raman Spectra Measured along a Profile Across the Fibril Main Axis. Insulin fibrils were grown at pH 2.5 and 70 °C as previously described.[23] According to SEM and AFM, the insulin fibrils have variable lengths with a width of 17−20 nm and a height of 8−10 nm, in agreement with previously reported results.[21,24] The majority of the fibrils exhibited a left-handed twist with a periodicity of 100 nm, as shown in the SEM images in Figure 1.

Tip-enhanced Raman spectroscopy (TERS) was used to structurally characterize the insulin fibril surface. The instrumental and experimental details of the TERS workflow described previously were used.[20] Insulin fibrils were immobilized on a glass slide, and TERS spectra were measured in 1-nm steps along a fibril cross section, as shown in Figure 2. This step size was used according to previous results and showed a lateral resolution of a similar range.[20] A total of 29 TERS spectra were acquired (see Figures S1a and S2 in SI for all raw data), which are called a "single fibril data set" therein. The majority of the raw TERS spectra exhibited high signal-to-noise ratios with clearly distinguishable Raman bands. In order to exclude contamination of the probes, background measurements were repeatedly performed.[22]

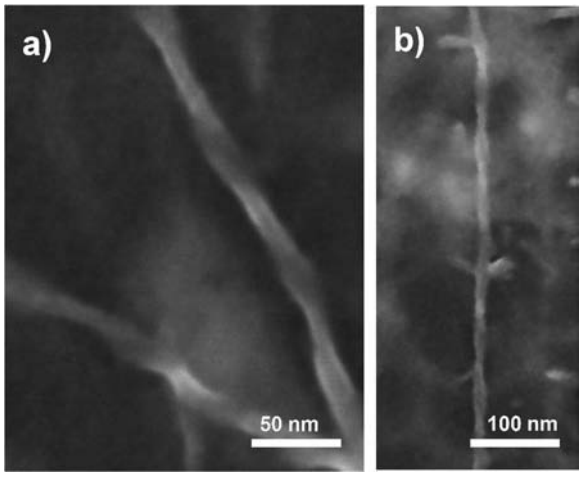

Figure 1. Morphology of insulin fibrils. SEM images reveal a left-handed twist.

A protein Raman spectrum is typically composed of contributions from three major types of vibrational modes, which originate from the polypeptide backbone (amide bands) and aromatic and nonaromatic amino acid residue side chains. The positions of the amide I bands, which depend on the conformation of the polypeptide backbone and intra- and intermolecular hydrogen bonds, are indicators of the protein secondary structure.[25] One of the main goals of this study was to understand the fibril surface structure; therefore, all of the acquired TERS spectra were classified on the basis of the positions of the amide I bands. Protein secondary structures were assigned as β-sheets if the maxima of the amide I bands were between 1664 and 1678 cm^{-1}. Amide I bands with maxima between 1640 and 1664 cm^{-1} were assigned to α-helical/unordered protein structures.[26] TERS spectra with broad amide I bands that spread over α-helical and β-sheet regions or had two peaks of comparable intensities at 1640−1655 cm^{-1} and 1664−1678 cm^{-1} were then grouped separately and considered as mixtures of all of the protein secondary structures described above.

Amide III bands are also sensitive to the polypeptide backbone conformation.[25] However, amide III bands are less informative for determining a protein's secondary structure than amide I bands because the amide III spectral range (1230−1300 cm^{-1}) overlaps strongly with side chain contributions, including CH_2 and C−C vibrations.

TERS measurements across the main fibril axis demonstrated that β-sheet structures dominated one fibril side, whereas another fibril side was composed of mixtures of α-helix/unordered and β-sheet structures (Figure 2 and Figure S2 [SI]). Notably, β-sheet areas stretched over 12 nm of the fibril surface, indicating that this conformation covers a significant area of the fibril surface. Intriguingly, only half of the fibril surface line is dominated by pure β-sheet structure, whereas mixtures of α-helix/unordered and β-sheet structures are present on the other half. Only one TERS spectrum exhibited a pure α-helix/unordered conformation that interrupted the β-sheet cluster (point 28 in Figure 2). Thus, TERS spectra recorded along a single line perpendicular to the main fibril axis may have revealed two distinct parts of the surface, which may result from a fibril twist. To verify this hypothesis, future experiments would include two-dimensional TERS mapping of the fibril surface and spatial overlapping of TERS data with a high-resolution AFM image of the same fibril, which reveals clearly the fibril topology. Typical AFM images of individual fibrils obtained using cantilevers modified for TERS measurements can be found in the SI section (Figure S1). These AFM images lack a high quality because of the attached (rough) silver particle (diameter about 20−30 nm) to a typical AFM tip. Nevertheless the topographies clearly show the characteristics of fibrils and give their main dimensions, while they do not reveal any detailed morphology.

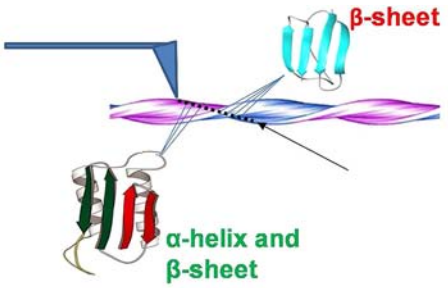

	1	2	3	4	5	6	7	8	9	10	11	12	13	14	15	16	17	18	19	20	21	22	23	24	25	26	27	28	29
Amide I																													
Cys													+					+	+	+	+	+	+	+	+	+	+	+	+
Tyr																				+	+	+	+	+	+	+	+	+	+
Phe		+	+	+	+						+																		
His						+	+				+	+	+																
Pro						+				+	+																		

Figure 2. Schematic illustration of the scan direction along the fibril profile (top) and graph (bottom) showing changes in the protein secondary structure (first row) and amino acid residue composition. β-Sheets, α-helix/unordered, and mixed protein structures are shown in red, blue, and green, respectively. TERS spectra with suppressed amide I bands are shown in black. The black dotted line indicates the center of the fibril. The presence of characteristic bands for Cys, Tyr, Phe, His, and Pro in the spectrum are marked by a "+". The corresponding spectra are given in Figure S2, SI.

Despite this limitation of the current TERS instrumentation, characterization of the structure and amino acid residue composition of the fibril surface is feasible. Here we report on an average of a large number of TERS spectra acquired from many individual fibril surfaces. This analysis allowed us to address both the secondary structure and amino acid residue composition of the fibril surface and demonstrate a significant difference relative to the fibril core (see below). It is noteworthy, that rinsing the substrate surface and adsorbed fibrils with acidic water before drying (see Materials and Methods) should ensure the removal of all nonaggregated insulin. High-resolution AFM images (not shown) do not show any irregularities associated with insulin molecules adsorbed on the surface of fibrils. The studied specimens were carefully selected to ensure all TERS spectra were collected on insulin fibrils and not on unordered aggregates or individual protein molecules. Prior to TERS measurements, several AFM images of different sizes were collected from each individual fibril to check its characteristic dimensions (length, height, and width).

In addition to providing information about the protein secondary structure, which is evident from the positions of amide I bands, Raman spectroscopy can also be used to identify specific amino acid residues.[20,27,28] Amino acid residues can be identified on the basis of the characteristic Raman bands of its side chains (summarized in Table S1 in the SI).[20,28] The contribution of $COOH/COO^-$ and NH_2^+/NH_3^+ groups to the TERS spectra was also evident in the Raman spectra. However, we did not assign amino acid residues referring to saturated hydrocarbon side chains, such as alanine, valine, leucine, and isoleucine, because their spectral signatures strongly overlap, and an unambiguous distinction was not possible.

The analysis of all 29 TERS spectra from the single fibril data set (Figure 2 and Figure S2, in the SI) indicated that Cys and Tyr residues are primarily present in areas dominated by β-sheets. Phe was often observed in areas with mixtures of α-helix and β-sheet structures. Pro was present in areas with α-helices and mixtures of α-helix and β-sheet structures but not in areas with pure β-sheet structures. Furthermore, Tyr was present alongside with Cys, whereas Phe was located on the opposite side of the fibril surface, where neither Cys nor Tyr were evident. These results demonstrate that amino acids are preferentially present in areas with a specific type of protein secondary structure.

Although the 29 TERS spectra acquired along one cross section represent a relatively small data set, important conclusions about the heterogeneity of the fibril surface and cluster organization can be made. In the following sections, it is demonstrated that further measurements of the surface of eight insulin fibrils confirm these results. TERS spectra were collected with a step size between 0.5 to 10 nm to characterize larger surface areas, and a total of 162 spectra from all nine fibrils ("multiple fibril data set" therein) were utilized for the analysis. The analysis of the spectra indicated that the fibril surface was highly heterogeneous. Almost half (88 spectra) of the TERS spectra displayed a suppressed amide I band (details in Table S2, in the SI, and representative spectra in Figure S3, in the SI). The absence of amide I bands in surface-enhanced Raman spectra has already been observed in previous studies of biological samples.[29] The exact interpretation of this phenomenon is not relevant here and does not affect further discussion.

TERS spectra with intense amide I bands (74 spectra total) were assigned to one of three groups according to their amide I band position, as described above. These groups included TERS spectra dominated by β-sheet structures (20 spectra), a mixture of α-helical and unordered structures (41 spectra), and a mixture of all secondary structural conformations (13 spectra). Selected TERS spectra from each group are shown in Figure 3. We used these TERS spectra also to analyze the amino acid residue compositions of the α-helix/unordered and pure β-sheet regions (Figure 4).

On the basis of the collected data, the insulin fibril surface is found to contain approximately 55% α-helical and unordered protein structures, whereas approximately 34% of the surface is dominated by pure β-sheet protein structures. Approximately 11% of the analyzed TERS spectra indicate a mixture of β-sheet, α-helical, and unordered protein structures. It is

dx.doi.org/10.1021/ja303263y | J. Am. Chem. Soc. 2012, 134, 13323−13329

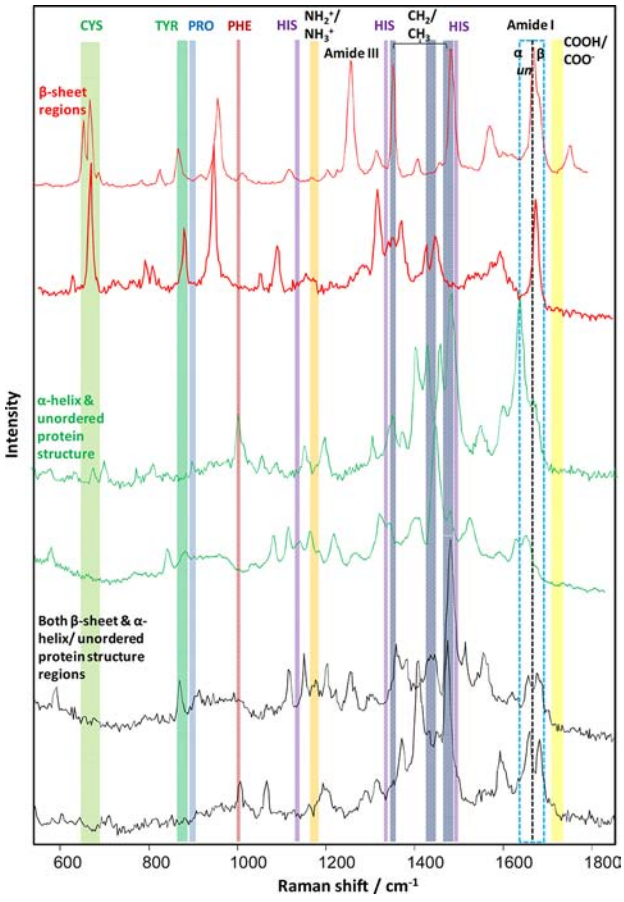

Figure 3. Representative insulin fibril TERS spectra assigned to one of three groups according to the dominant protein secondary structure revealed by amide I bands (See Figure S2, in the SI, for the complete set). β-sheet clusters (red), α-helix/unordered regions (green) and mixed regions with significant contributions from all secondary structures (black) are shown. Specific amino acid vibrational modes are marked with colored lines. Amide I and III bands are marked with dashed lines, showing the borders between protein secondary structures. NH_2^+/NH_3^+ (1144 cm^{-1}) and $COOH/COO^-$ (1687–1700 cm^{-1}) vibrational modes are also indicated.

noteworthy that this secondary structural composition differs from that found for the single fibril data set (Figure 2). As the single fibril data set (about 20% of the multiple fibril data set) was acquired along a single line for a single fibril, it is only reasonable that the characteristics of this small subset are not representative for a larger number of fibrils. The latter further indicates a strong heterogeneity of the fibril surface.

DISCUSSION

Amino Acid Propensities for Various Protein Secondary Structures on the Fibril Surface. Our results confirm the recently published data of Deckert-Gaudig et al., which demonstrated the presence of α-helical structures on the surface of insulin fibrils.[30] The presence of α-helices is not evident in "bulk" Raman spectra of insulin fibrils, indicating that its relative contribution is small.[11] In a previous study, we examined the structure of insulin fibrils by deep UV resonance Raman spectroscopy and determined that the contribution of α-helical and unordered protein structures is practically negligible.[13,23] However, the significant contribution of α-helical and unordered protein structures in TERS spectra

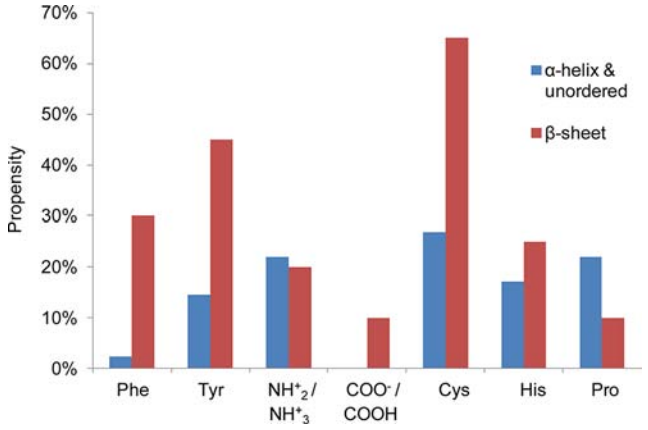

Figure 4. Relative propensity plot of amino acid residues for β-sheet (red) and α-helix/unordered (blue) structures. To obtain the relative propensity, the number of spectra containing a specific amino acid residue (Table S1, SI) was divided by the total number of TERS spectra in each group (41 for α-helix/unordered regions and 20 for β-sheet regions). The resulting value was then multiplied by 100 to obtain a percentage.

indicates their predominant localization on the fibril surface. The latter *qualitative* conclusion is well supported by the experiment despite a significant heterogeneity of the fibril surface. Only a part of the fibril surface is similar to the β-sheet dominated fibril core; the remainder is clearly of α-helical or random structure. The presented characterization of the fibril surface secondary structure and surface amino acid residue composition provides even (semi-)*quantitative* information. The latter is currently limited by somewhat unclear differentiation between the surface and the core determined by the specific depth resolution of TERS, as well as by the specific and yet unknown surface enhanced Raman cross sections.

The significant presence of β-sheet structures on the surface of insulin fibrils is somewhat surprising because, according to Dobson et al.,[21,31] the β-rich fibril core is wrapped by an unordered protein structure. Consequently, one would expect the β-sheet core to be buried inside the fibril and that the β-sheet structures would not play any role in fibrillar toxicity and propagation. However, on the basis of the substantial presence of β-sheet structures on the surface of insulin fibrils, we speculate that these unprotected β-sheet areas could be responsible for templating the formation of new protofilaments and protofibrils and for the intertwining process as proposed by Winter et al.[32] The latter work has shown that prefibrillar aggregates tend to cluster around fibrils formed earlier. In addition, Milhiet et al. found by using high-speed AFM (HS-AFM) that a new protofibril often grows on the surface of another protofibril and almost completely replicates its shape. This elongation process occurs in one direction and appears to be very rapid (a few tens of nanometers per second).[33] Obviously, the discovery of a considerable amount of β-sheet on the surface of insulin fibrils agrees with Milhiet's observations and provides additional information for understanding the mechanism of the amyloid fibrillation process.

The analysis of the contribution of the aromatic amino acids Tyr and Phe demonstrates that both amino acid residues are frequently present on the surface of insulin fibrils. These results are consistent with our prior deep UV resonance Raman spectroscopy observations, which indicated that Tyr and Phe in insulin fibrils are exposed to aqueous media.[34,35] The TERS

data demonstrate that the probability of finding Phe in a β-sheet area is more than 12 times higher than that in an α-helix/unordered protein area. Intriguingly, in globular proteins, the relative propensity of Phe for β-sheet areas is also higher than that for α-helical regions and turns.[36] Gazit recently proposed that aromatic interactions may play a key role in fibril proliferation.[37] Furthermore, phenylalanine has been reported to play a significant role in protein aggregation.[38] Thus, the high propensity of phenylalanine for β-sheet regions of the insulin fibril surface is consistent with its suggested role in the amyloid fibrillation process.

In addition to Phe, Tyr was approximately 3.1 times more prevalent in β-sheet areas than in α-helical regions of the insulin fibril surface (Figure 4). These results are also consistent with previous findings, indicating that the Tyr distribution in a fibril depends on the pH during protein aggregation.[23] At pH 2.1 and higher, Tyr is predominantly located on the fibril surface and is accessible to the solvent. However, if fibrils are formed below pH 2.1, Tyr is packed inside the fibril core. These results expand upon the current knowledge of Tyr distribution and demonstrate that Tyr is not equally distributed between β-sheet and α-helical regions on the fibril surface.

The characteristic proline ring-stretching mode made a noticeable contribution to the TERS spectra but was not evident in the bulk Raman spectra of insulin fibrils, indicating that Pro is primarily located on the fibril surface. In globular proteins, Pro has the highest propensity for turns and unordered loops and is known to break both β-sheet and α-helical segments due to its structural characteristics.[36,39] Thus, our detection of Pro indicates the presence of turns and loops on the fibril surface. According to our data, proline is 2-fold more abundant in α-helix/unordered clusters (20% probability) than in β-sheet areas (10% probability). In TERS spectra, unordered secondary structures almost always coexist with α-helical structures, and the high probability of Pro in the α-helix/unordered group may originate from these unordered secondary structures. Although there is only one Pro residue in the insulin sequence, the Pro marker band was evident in every sixth TERS spectra. Pro is most likely located on the edges of β-sheets or α-helices (see Discussion below). The protein fibrillation process has a complex mechanism and is associated with dramatic secondary structure changes. Understanding the structure of the fibril core has fueled a new area of research. The distribution of amino acid residues in the fibril core and on the surface is also a critical question that can be addressed by TERS data. Figure S4 (SI) shows the relative appearance of certain amino acid residues on the fibril surface relative to their overall number in the insulin sequence. For example, Pro exhibits a high tendency to be present on the fibril surface (40%; Figure S4 [SI]). The propensity of Pro for both α-helical and β-sheet conformations has been reported to be extremely low in globular proteins, which is attributed to the ability of Pro to disrupt both of these conformations.[36,39] Furthermore, the fibril core has been reported to be a well-ordered β-sheet structure.[40] Thus, the presence of Pro in the fibril core would most likely disrupt the β-sheet structure.

Raman bands at 1187, 1335, and 1495 cm^{-1} could be assigned to the histidine side chain.[20] According to the TERS spectra collected, histidine has an almost equal presence in both α-helix/unordered (17%) and β-sheet (25%) regions.

In native insulin, six cysteine residues form three disulfide bonds (Figure S5, SI). The TERS signature of cysteine is typically composed of several strong bands between 600 and 668 cm^{-1}.[28] Due to the possible rotation around these S−S bridges, the number of detected signals in the TERS spectra of insulin varies as shown in Figure 2. On the basis of the analysis of the data presented in Figure 3, the propensity of Cys for β-sheet structures is found to be almost 2.5 times higher than that for α-helix/unordered regions, in contrast to globular proteins, in which cysteine has a higher propensity for α-helicies.[36]

Charge Distribution on the Fibril Surface. TERS spectra were evaluated with regard to the charge distribution associated with carboxylic acid and amino groups. Primary amines in the side chains of asparagine (Asn), glutamine (Gln), arginine (Arg), and lysine (Lys) and the N-terminal groups of Gly and Phe are protonated at pH 2.5,[41] providing positive charges. While NH_2^+/NH_3^+ groups have nearly identical propensities for β-sheet regions (20%) and α-helix/unordered areas (22%), $COOH/COO^-$ groups are absent in α-helix/unordered regions. Some $COOH/COO^-$ groups (8%) were found on the surface of β-sheet clusters. However, their presence is very low (8%) compared with that of NH_2^+/NH_3^+ groups (42%). The carboxyl groups of Asn and Thr have pK_a values of approximately 3.6[42] and are significantly protonated at pH 2.5. Moreover, the side chain of glutamine has a pK_a value of 3.9 and also remains protonated at pH 2.5. Thus, amino and imino groups are relatively abundant on the fibril surface compared with carboxyl groups and are almost equally distributed across α-helix/unordered β-sheet regions. The application of classical tools for surface charge determination, such as the Kelvin probe force and AFM, is limited in the case of amyloid fibrils due to the weak charge of these surfaces, and thus, the use of TERS to characterize the charge of the fibril surface represents a significant advance. The surface charges of filaments and fibrils play a crucial role in protofilament intertwining, fibril morphology, and chirality.[23] For example, insulin aggregation below pH 2.1 has been recently shown to lead to the formation of flatlike fibrils. However, left-handed fibrils grow when the aggregation pH is above 2.4. These flatlike and left-handed fibrils have opposite supramolecular chirality according to VCD spectra.[43] Furthermore, small increases in pH have been reported to cause the spontaneous reconfiguration of mature flatlike fibrils into left-handed fibrils.[43] The pH-dependent insulin fibril polymorphism may be caused by the protonation/deprotonation of amino acid residue side chains with a pK_a close to 2.4.[23] These protonation/deprotonation processes most likely occur on the surface of insulin protofilaments.

Hydrophobicity of the Fibril Surface. The surface hydrophobicity is expected to play a significant role in fibril biological activity and associated toxicity. From the obtained data the hydrophobicity of fibril surfaces can be estimated as follows. Many hydrophobic amino acids, such as Val and Leu, have aliphatic side chains. At the same time, most of the amino acids in the insulin sequence, including the hydrophilic ones such as Cys or His, also have one or several CH_2 groups. Therefore, TERS has a certain limitation in differentiating hydrophobic and hydrophilic amino acids unless the amino acid residue is identified on the basis of the TERS signature. Alternatively, the estimation of the surface polarity could be made on the basis of TERS data by evaluating the number of amino and carboxyl groups. As discussed above, 8% of all acquired TERS spectra showed the presence of $COOH/COO^-$ groups and 42% of NH_2^+/NH_3^+ groups. Therefore, 50% of the spectra showed the presence of hydrophilic groups. One can expect that the rest 50% of the recorded spectra originate from

the hydrophobic areas. Remarkably, these TERS data are quite consistent with the hydrophilic/hydrophobic distribution of amino acids on the insulin fibril surface determined by a different analytical approach.[44] In that study, NMR coupled with hydrogen−deuterium exchange has been utilized to determine amino acid residues that are not accessible to the solvent and, consequently, located in the fibril core. The rest of the amino acid residues are expected to be located on the fibril surface and be solvent accessible. Intriguingly, the half of these amino acids is hydrophilic and the other half is hydrophobic,[44] which is in agreement with the TERS data reported here.

■ CONCLUSIONS

We performed a detailed characterization of the insulin fibril surface by determining its amino acid residue composition and protein secondary structure. The fibril surface is strongly heterogeneous, consisting of α-helical, unordered, and β-sheet areas as well as mixtures of these conformations. According to our data, only ∼34% of the surface is dominated by pure β-sheet structures, while the rest of it is composed of α-helix and unordered protein structures (∼55%). The tendency of specific amino acid residues to be on the fibril surface and specific secondary structures to be on the surface was evaluated. Our data indicate that carboxyl, amino, and imino groups are almost equally distributed over β-sheet and α-helix/unordered regions. Overall, this study provides valuable new information about the structure and composition of the insulin fibril surface and demonstrates the power and great potential of TERS for fibril characterization. This is one of the first comprehensive reports on the use of TERS to examine amyloid fibrils. Although significant novel information has been obtained about fibril surface structure and composition, many questions remain. We envision a significant expansion of the use of TERS in the characterization of various protein aggregates, including amyloid fibrils and fibril polymorphs as well as fibrillation intermediates, such as protofilaments and protofibrils. The latter will be extremely valuable for understanding the general fibrillation mechanism and protofibril intertwining.

■ ASSOCIATED CONTENT

Supporting Information

Figures S1−S5 and Tables S1 and S2. This material is available free of charge via the Internet at http://pubs.acs.org.

■ AUTHOR INFORMATION

Corresponding Author

ilednev@albany.edu

Notes

The authors declare no competing financial interest.

■ ACKNOWLEDGMENTS

We thank Dr. Vitaly Sikirzhytski for his help with spectral data treatment. This project is supported by Award Number R01AG033719 from the National Institutes of Health (I.K.L.).

■ REFERENCES

(1) Dobson, C. M. *Nature* **2003**, *426*, 884−890.
(2) Brenner, D. A.; Jain, M.; Pimentel, D. R.; Wang, B.; Connors, L. H.; Skinner, M.; Apstein, C. S.; Liao, R. *Circ. Res.* **2004**, *94*, 1008−1010.
(3) Clark, A.; Charge, S. B.; Badman, M. K.; MacArthur, D. A.; de Koning, E. J. *Biochem. Soc. Trans.* **1996**, *24*, 594−599.
(4) Westermark, P.; Eriksson, L.; Engstrom, U.; Enestrom, S.; Sletten, K. *Am. J. Pathol.* **1997**, *150*, 67−73.
(5) Dische, F. E.; Wernstedt, C.; Westermark, G. T.; Westermark, P.; Pepys, M. B.; Rennie, J. A.; Gilbey, S. G.; Watkins, P. J. *Diabetologia* **1988**, *31*, 158−161.
(6) Lindquist, S. L.; Kelly, J. W. *Cold Spring Harbor, Perspect. Biol.* **2011**, *3*, a004507.
(7) Paravastu, A. K.; Leapman, R. D.; Yau, W. M.; Tycko, R. *Proc. Natl. Acad. Sci. U.S.A.* **2008**, *105*, 18349−18354.
(8) Ivanova, M. I.; Sievers, S. A.; Sawaya, M. R.; Wall, J. S.; Eisenberg, D. *Proc. Natl. Acad. Sci. U.S.A.* **2009**, *106*, 18990−18995.
(9) Paravastu, A. K.; Petkova, A. T.; Tycko, R. *Biophys. J.* **2006**, *90*, 4618−4629.
(10) Jaroniec, C. P.; MacPhee, C. E.; Bajaj, V. S.; McMahon, M. T.; Dobson, C. M.; Griffin, R. G. *Proc. Natl. Acad. Sci. U.S.A.* **2004**, *101*, 711−716.
(11) Dong, J.; Wan, Z.; Popov, M.; Carey, P. R.; Weiss, M. A. *J. Mol. Biol.* **2003**, *330*, 431−442.
(12) Ortiz, C.; Zhang, D.; Ribbe, A. E.; Xie, Y.; Ben-Amotz, D. *Biophys. Chem.* **2007**, *128*, 150−155.
(13) Oladepo, S. A.; Xiong, K.; Hong, Z.; Asher, S. A.; Handen, J.; Lednev, I. K. *Chem. Rev.* **2012**, *112*, 2604−2628.
(14) Hartschuh, A. *Angew. Chem., Int. Ed.* **2008**, *47*, 8178−8191.
(15) Deckert-Gaudig, T.; Deckert, V. *Curr. Opin. Chem. Biol.* **2011**, *15*, 719−724.
(16) Stadler, J.; Schmid, T.; Zenobi, R. *Nanoscale* **2012**, *4*, 1856−1870.
(17) Richter, M.; Hedegaard, M.; Deckert-Gaudig, T.; Lampen, P.; Deckert, V. *Small* **2011**, *7*, 209−214.
(18) Bohme, R.; Cialla, D.; Richter, M.; Rosch, P.; Popp, J.; Deckert, V. *J. Biophotonics* **2010**, *3*, 455−461.
(19) Cialla, D.; Siebert, R.; Hubner, U.; Moller, R.; Schneidewind, H.; Mattheis, R.; Petschulat, J.; Tunnermann, A.; Pertsch, T.; Dietzek, B.; Popp, J. *Anal. Bioanal. Chem.* **2009**, *394*, 1811−1818.
(20) Deckert-Gaudig, T.; Kämmer, E.; Deckert, V. *J. Biophotonics* **2012**, *5*, 215−219.
(21) Jimenez, J. L.; Nettleton, E. J.; Bouchard, M.; Robinson, C. V.; Dobson, C. M.; Saibil, H. R. *Proc. Natl. Acad. Sci. U.S.A.* **2002**, *99*, 9196−9201.
(22) Jansen, R.; Dzwolak, W.; Winter, R. *Biophys. J.* **2005**, *88*, 1344−1353.
(23) Budich, C.; Neugebauer, U.; Popp, J.; Deckert, V. *J. Microsc.* **2008**, *229*, 533−539.
(24) Khurana, R.; Ionescu-Zanetti, C.; Pope, M.; Li, J.; Nielson, L.; Ramirez-Alvarado, M.; Regan, L.; Fink, A. L.; Carter, S. A. *Biophys. J.* **2003**, *85*, 1135−1144.
(25) Carey, P. R. *Biochemical Applications of Raman and Resonance Raman Spectroscopies*; Academic Press: New York, 1982.
(26) Fabian, H.; Anzenbacher, P. *Vib. Spectrosc.* **1993**, *4*, 125−148.
(27) Deckert-Gaudig, T.; Deckert, V. *J. Raman Spectrosc.* **2009**, *40*, 1446−1451.
(28) Deckert-Gaudig, T.; Deckert, V. *Small* **2009**, *5*, 432−436.
(29) Podstawka-Proniewicz, E.; Piergies, N.; Skoluba, D.; Kafarski, P.; Kim, Y.; Proniewicz, L. M. *J. Phys. Chem. A* **2011**, *115*, 11067−11078.
(30) Deckert-Gaudig, T.; Deckert, V. *Phys. Chem. Chem. Phys.* **2010**, *12*, 12040−12049.
(31) Jimenez, J. L.; Guijarro, J. I.; Orlova, E.; Zurdo, J.; Dobson, C. M.; Sunde, M.; Saibil, H. R. *Embo J.* **1999**, *18*, 815−821.
(32) Jansen, R.; Dzwolak, W.; Winter, R. *Biophys. J.* **2005**, *88*, 1344−1353.
(33) Milhiet, P. E.; Yamamoto, D.; Berthoumieu, O.; Dosset, P.; Le Grimellec, C.; Verdier, J. M.; Marchal, S.; Ando, T. *PLoS One* **2010**, *5*, e13240.
(34) Aoyama, M.; Kurihara, K.; Shibata, K. *Biochim. Biophys. Acta* **1965**, *107*, 257−265.
(35) Smith, G. D.; Pangborn, W. A.; Blessing, R. H. *Acta Crystallogr., Sect. D* **2005**, *61*, 1476−1482.
(36) Chou, P. Y.; Fasman, G. D. *Biochemistry* **1974**, *13*, 211−222.
(37) Gazit, E. *FEBS J.* **2005**, *272*, 5971−5978.

(38) Aitken, J. F.; Loomes, K. M.; Konarkowska, B.; Cooper, G. J. *Biochem. J.* **2003**, *374*, 779−784.
(39) Myers, J. K.; Pace, C. N.; Scholtz, J. M. *Biochemistry* **1997**, *36*, 10923−10929.
(40) Xu, M.; Shashilov, V.; Lednev, I. K. *J. Am. Chem. Soc.* **2007**, *129*, 11002−11003.
(41) Hefford, M. A.; Oda, G.; Kaplan, H. *Biochem. J.* **1986**, *237*, 663−668.
(42) Darrington, R. T.; Anderson, B. D. *J. Pharm. Sci.* **1995**, *84*, 275−282.
(43) Kurouski, D.; Dukor, R. K.; Lu, X.; Nafie, L. A.; Lednev, I. K. *Chem. Commun.* **2012**, *48*, 2837−2839.
(44) Kurouski, D.; Washington, J.; Ozbil, M.; Prabhakar, R.; Shekhtman, A.; Lednev, I. K. *PloS One* **2012**, *7*, e36989.